We are IntechOpen,
the world's leading publisher of
Open Access books
Built by scientists, for scientists

6,500
Open access books available

176,000
International authors and editors

190M
Downloads

Our authors are among the

154
Countries delivered to

TOP 1%
most cited scientists

12.2%
Contributors from top 500 universities

CLARIVATE ANALYTICS
BOOK CITATION INDEX
INDEXED

WEB OF SCIENCE™

Selection of our books indexed in the Book Citation Index
in Web of Science™ Core Collection (BKCI)

Interested in publishing with us?
Contact book.department@intechopen.com

Chapter

Interferometric Phase Transmitarray for Millimeter-Wave MIMO System

Yu Luo and Xiaoxuan Guo

Abstract

A millimeter-wave (mmW) interferometric phase transmitarray for the multiple-input multiple-output (MIMO) system is proposed, and its phase distribution is the interference superposition of electromagnetic waves radiated by two patch antennas at different locations. Its characteristic is that when multiple EM waves illuminate the center of the array, the transmitted waves are formed into high-directivity beams. In addition, when the plane wave illuminates the interference phase transmitarray vertically, the transmissive plane wave will be scattered and focused to two different positions. A novel MIMO system can be implemented based on the above two characteristics. Compared with the conventional lens MIMO, the advantage of the MIMO system integrated by the interferometric phase transmitarray is that multiple antennas can share one transmitarray, which is beneficial to the miniaturization of the MIMO transceiver. More critically, all channels can efficiently transmit information and increase channel capacity.

Keywords: interferometric phase, transmitarray, MIMO, miniaturization, channel capacity

1. Introduction

Recently, mmW technology has been the top priority of the fifth-generation (5G) wireless network [1]. Multiple-input multiple-output (MIMO) has been recognized as the most effective application of 5G technology since it can increase the data transmission rate by expanding channel capacity [2]. Generally, elements in MIMO antennas are with wider beamwidth to ensure that each receiving antenna can receive the signals from each transmitting antenna. However, for mmW antennas, high-gain and narrower beamwidth antennas are employed to overcome channel fading. With high gain elements, conventional lens-based 2×2 MIMO systems are investigated [3–6] as shown in **Figure 1**. This kind of MIMO system requires multiple lenses, which is not conducive to the miniaturization of the MIMO transceiver. Moreover, the signals of Channel 1 and Channel 2 are robust and easy to be received, but the signals of Channel 3 and Channel 4 are weak and unable to transmit information effectively due to the narrow beamwidth of the elements. Besides, MIMO systems in the mmW band have
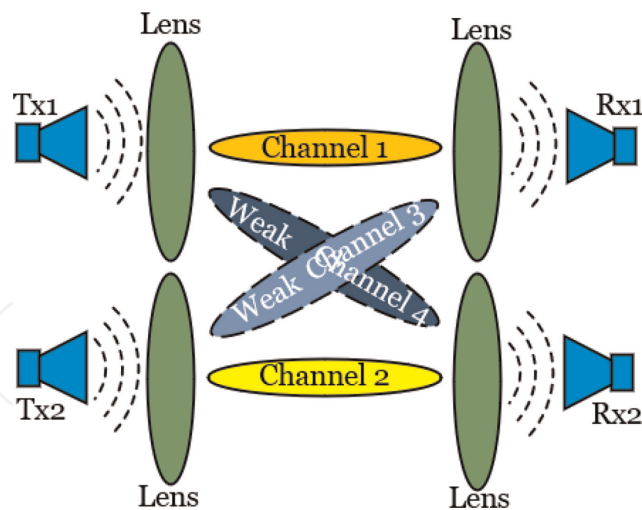
Figure 1.
The 2 × 2 MIMO system integrated by the conventional lens.

high requirements for antenna and circuit performance, which leads to high costs and complexity [7–9].

Current metamaterials have the characteristics of flexible control of electromagnetic (EM) waves and are widely used in mmW systems, such as radar, satellite communications, and imaging [10]. Metamaterials and their derivatives also have the advantages of thin thickness, small size, and lightweight, which can effectively solve problems such as cost and loss [11–13]. More importantly, metamaterials are widely used in transmitting and reflective arrays to realize beamforming and beam steering [14–21], which lays the foundation for realizing the miniaturization of the MIMO transceiver.

This paper proposes an interferometric phase transmitarray for the MIMO system. Its characteristic is that when multiple EM waves radiate toward the array, all the EM waves are beamforming into beams with high directivity. When the plane wave illuminates the interference phase transmitarray vertically, the transmissive plane wave will be scattered and focused to two different positions. Based on the above two characteristics, a novel MIMO system can be implemented, as shown in **Figure 2**. Compared with the MIMO system in **Figure 1**, the advantage of this novel MIMO system is that two antennas can share one transmitarray, which is beneficial to the miniaturization of the MIMO transceiver. All four channels can efficiently transmit information and increase channel capacity.
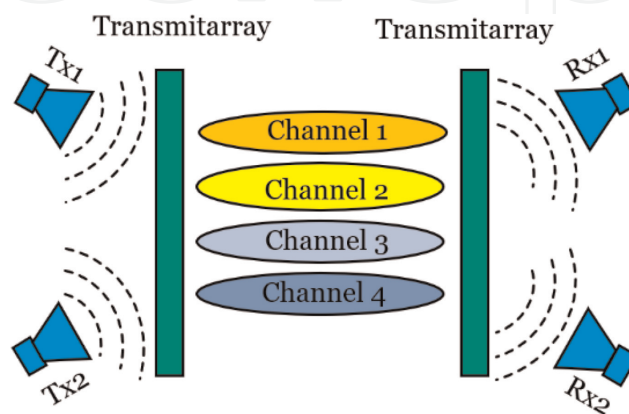

Figure 2.
The MIMO system integrated by the proposed lens.

2. Theoretical study

The theoretical study focuses on the phase distribution and incident field of the interferometric phase transmitarray.

2.1 The phase distribution

The ideal model of interferometric phase transmitarray is shown in **Figure 3**. Assuming the interferometric phase transmitarray is an N × N square array. When two EM waves are radiated by two feeds toward the array, the two transmitted EM waves are formed into a high-directivity beam.

For quantitative analysis, it is assumed that O_{mn} (x_m, y_n, 0) is the position of the unit cell in row m and column n. The coordinate of the Feed 1 (x_1, y_1, z_1). Here, for the convenience of calculation, the ideal point source model is selected for Feed 1. The phase distribution caused by the propagation path of the EM Wave 1 radiated by Feed 1 to the array is calculated by Eq. (1),

$$\phi_1(x_m, y_n) = k_0 \sqrt{(x_m - x_1)^2 - (y_n - y_1)^2 + z_1^2} \tag{1}$$

where $k_0 = 2\pi/\lambda_0$ is the wavenumber. To make the phase distribution of EM waves consistent passing through the transmitarray, the phase of the array itself should be $-\phi_1(x_m, y_n)$. Similarly, the phase distribution caused by the propagation path of the EM Wave 2 radiated by Feed 2 to the array is calculated by Eq. (2),

$$\phi_2(x_m, y_n) = k_0 \sqrt{(x_m - x_2)^2 - (y_n - y_2)^2 + z_2^2} \tag{2}$$

When Feed 1 and Feed 2 are excited together, the phase distribution of the array aperture is interferometric superimposed by Eq. (3),

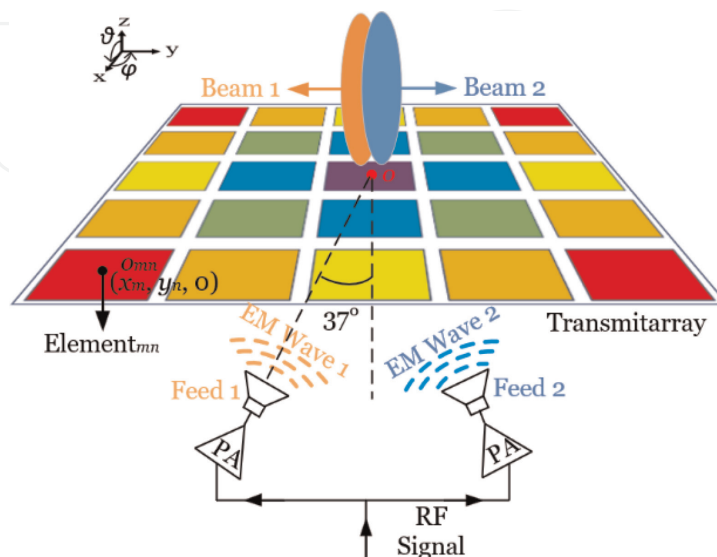$$\Delta\phi(x_m, y_n) = \arg(A_1(x_m, y_n) \exp(j\phi_1(x_m, y_n)) + A_2(x_m, y_n) \exp(j\phi_2(x_m, y_n))) \tag{3}$$

Figure 3.
The theoretical model of interferometric phase transmitarray. Reprinted with permission from Ref. [22]; copyright 2022 IEEE.
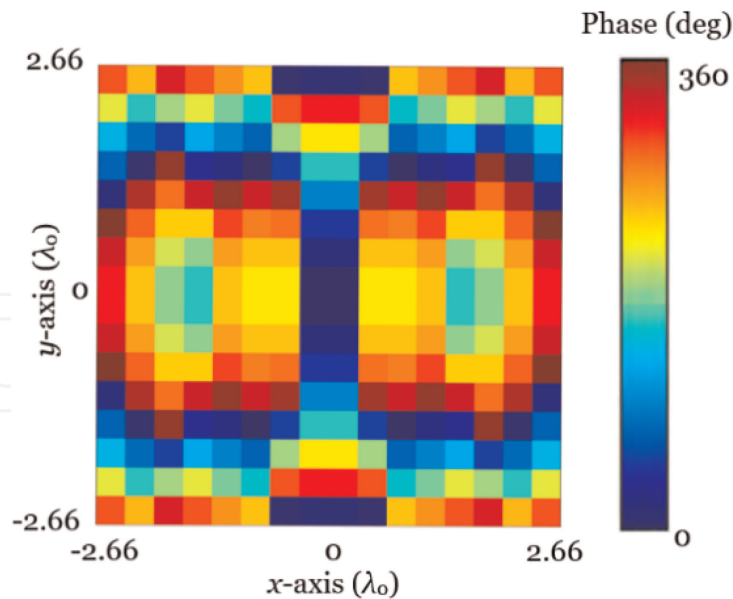
Figure 4.
The phase distribution of the interferometric phase transmitarray. Reprinted with permission from Ref. [22]; copyright 2022 IEEE.

where $A_1(x_m, y_n)$ and $A_2(x_m, y_n)$ are the amplitudes of E-field. To make the phase distribution of EM waves consistent through the transmitarray, the phase of the array itself should be $-\Delta\phi(x_m, y_n)$.

Establishing a MATLAB model. The two ideal point sources are set at $(-1.5\,\lambda_0, 0, -2\,\lambda_0)$ and $(1.5\,\lambda_0, 0, -2\,\lambda_0)$, and the phase distribution of the transmitarray is shown in **Figure 4**.

2.2 The incident field

Assume $f_{m,\,n}(\theta, \varphi)$ is the radiation pattern of the element in row m and column n, the radiation pattern of the transmitarray can be expressed as Eq. (4),

$$F(\theta, \varphi) = f_{m,n}(\theta, \varphi)S_a(\theta, \varphi) \tag{4}$$

where θ and φ are the elevation and azimuth angles. $S_a(\theta, \varphi)$ is expressed as Eq. (5),

$$S_a(\theta, \varphi) = \sum_{m=1}^{N}\sum_{n=1}^{N} \exp\left(-i\left(\phi\left(x_m, y_n\right) + kD\sin\theta \times \left((m - 1/2)\cos\varphi + (n - 1/2)\sin\varphi\right)\right)\right) \tag{5}$$

where l represents the length of the element. The phase $\phi(x_m, y_n)$ contains the phase of the unit itself $\phi_p(x_m, y_n)$ and the phase difference caused by the propagation distance $\phi_q(x_m, y_n)$. Furthermore, the directivity $Dir(\theta, \varphi)$ can be expressed as Eq. (6),

$$Dir(\theta, \varphi) = 4\pi|F(\theta, \varphi)|^2 / \int_0^{2\pi}\int_0^{\pi/2} |F(\theta, \varphi)|^2 \sin\theta d\theta d\varphi \tag{6}$$
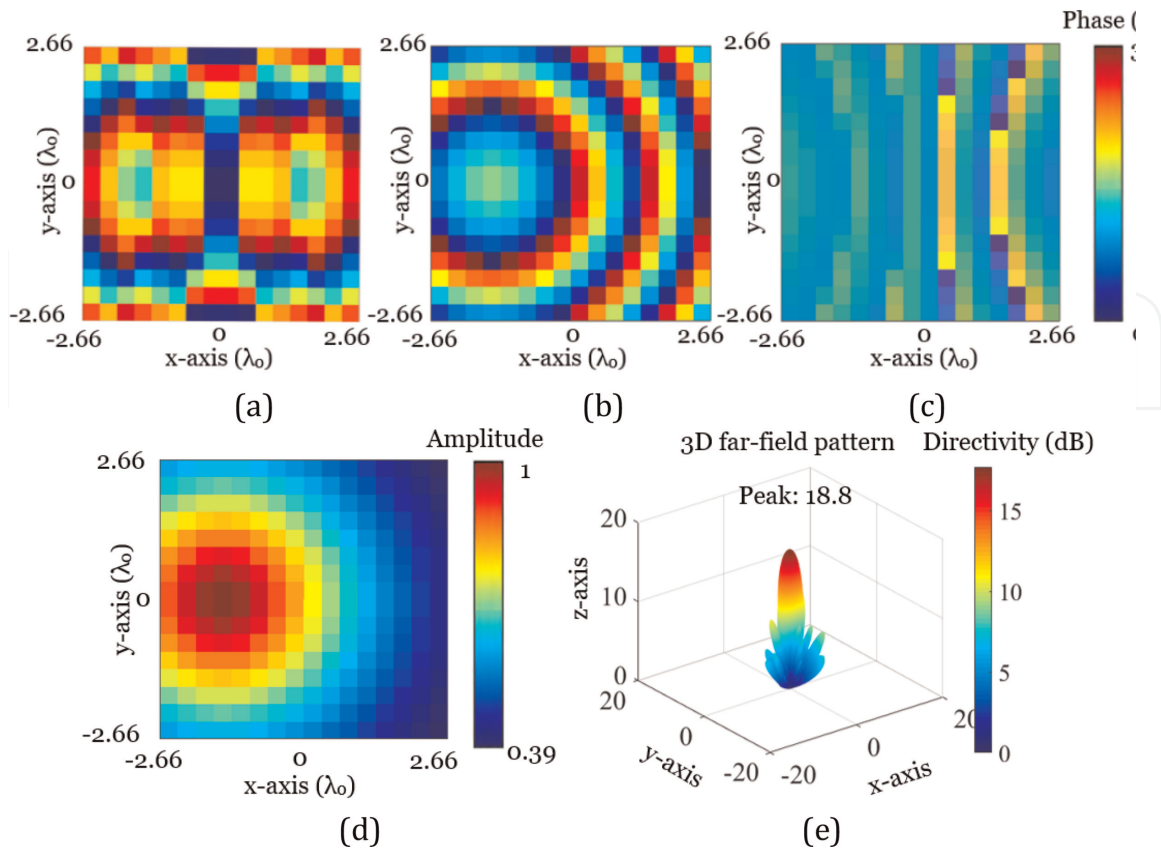
Figure 5.
The incident field analysis of Feed 1: (a) the phase distribution of the transmitarray itself, (b) the phase distribution caused by the propagation distance, (c) the superimposed phase distribution, (d) the amplitude distribution, and (e) the 3-D pattern. Reprinted with permission from Ref. [22]; copyright 2022 IEEE.

According to the above derivation, **Figure 5** shows the incident field of Feed 1. **Figure 5a** shows the phase distribution of the array itself, **Figure 5b** shows the phase distribution caused by the propagation distance, **Figure 5c** shows the superposition of **Figure 5a** and **Figure 5b**, **Figure 5d** shows the amplitude distribution, **Figure 5e** shows the 3-D pattern. Compared to **Figure 5b**, the phase distribution of **Figure 5c** is improved. Therefore, the beam shown in **Figure 5e** can achieve high directivity, and the peak is 18.8 dB.

Figure 6 shows the incident field analysis of Feed 2. **Figure 6a** shows the phase distribution of the array itself, **Figure 6b** shows the phase distribution caused by the propagation distance, **Figure 6c** shows the superposition of **Figure 6a** and **Figure 6b**, **Figure 6d** shows the amplitude distribution, **Figure 6e** shows the 3-D pattern. Compared to **Figure 6b**, the phase distribution of **Figure 6c** is improved. Therefore, the beam shown in **Figure 6e** can achieve high directivity, and the peak is 18.8 dB.

3. Realization of the interferometric phase transmitarray

The unit of the interferometric phase transmitarray is shown in **Figure 7**. The metal layer contains a square ring and patch as shown in **Figure 7a**. The overall structure is five dielectric and six metal layers arranged alternately, as shown in **Figure 7b**.
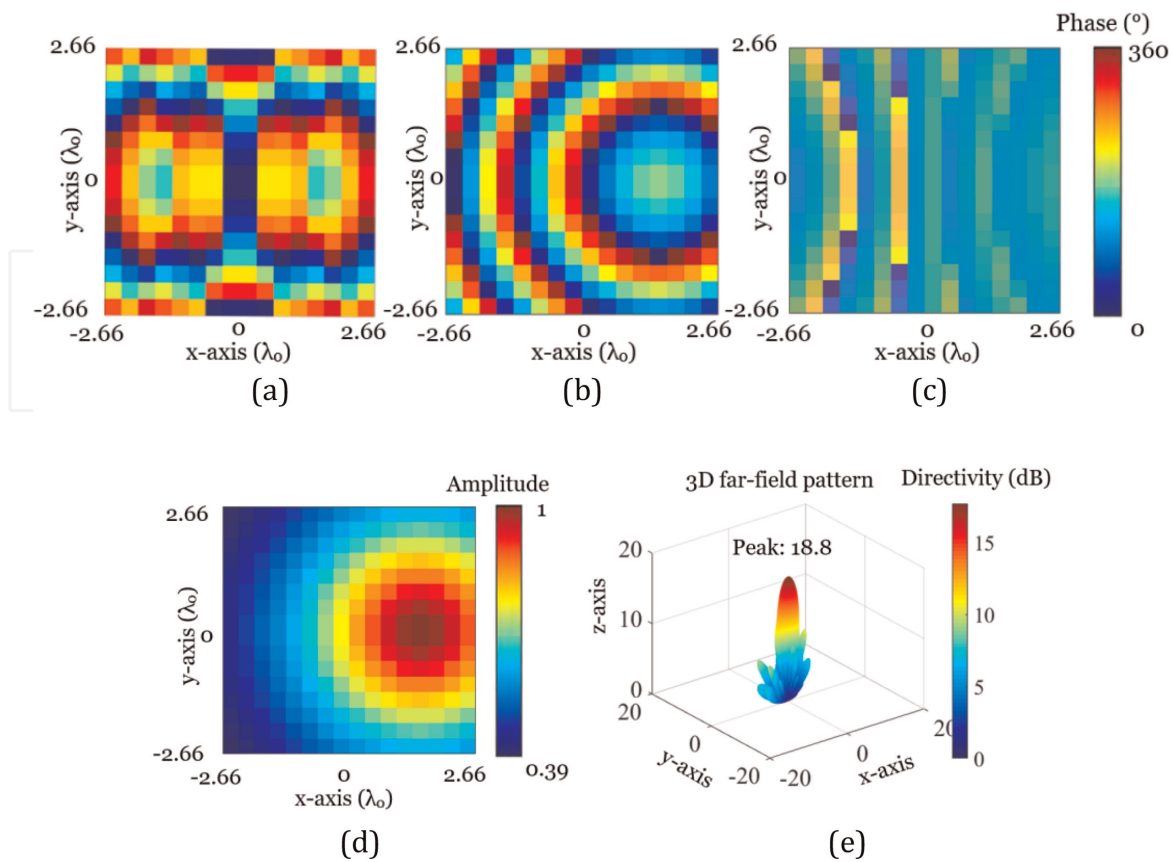
Figure 6.
The incident field analysis of Feed 2: (a) the phase distribution of the transmitarray itself, (b) the phase distribution caused by the propagation distance, (c) the superimposed phase distribution, (d) the amplitude distribution, and (e) the 3-D pattern. Reprinted with permission from Ref. [22]; copyright 2022 IEEE.
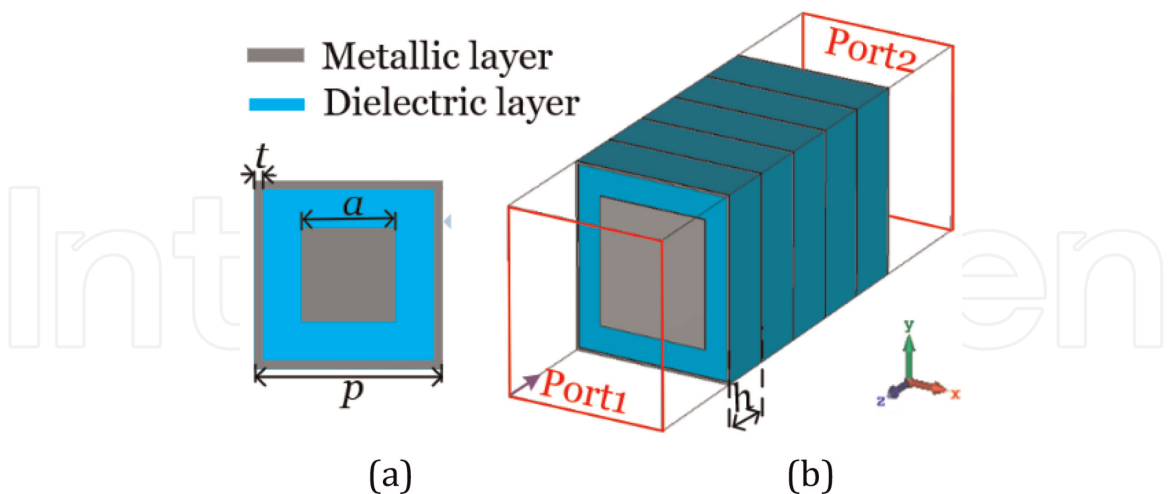

Figure 7.
The view of the unit. (a) Top view. (b) Overall view. Reprinted with permission from Ref. [22]; copyright 2022 IEEE.

The substrate adopts F4B, and its dielectric constant is 2.65. The thickness of the substrate is $h = 1.5$ mm. $p = 4$ mm is the unit period, and t equals 0.05 mm. Size a represents the side length of the square metal patch, which is related to the transmission characteristics of the unit. Eight units with different a are for comparison. **Figure 8a** shows that the phase change of the unit contains 300°. It can be seen from
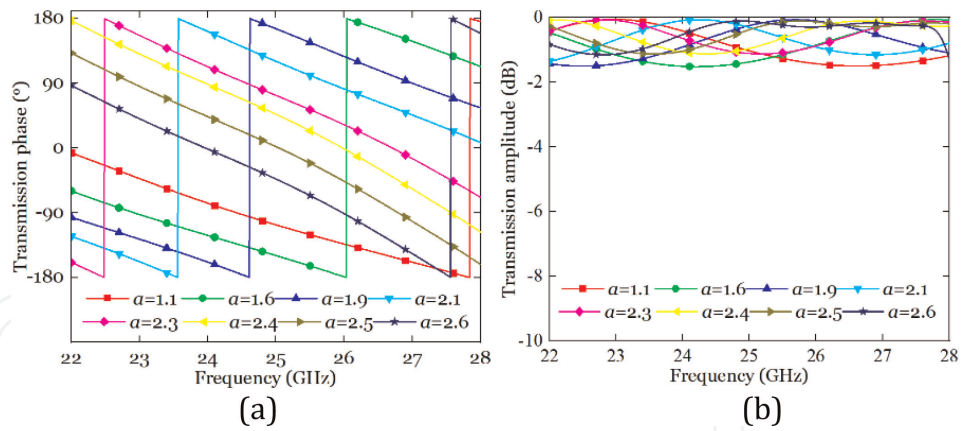
Figure 8.
Transmission characteristics of the unit: (a) phases, (b) amplitudes. Reprinted with permission from Ref. [22]; copyright 2022 IEEE.

Figure 8b that the transmission amplitude of the unit is higher than -2 dB, which indicates the EM waves can pass through the unit efficiently.

Utilize s a patch antenna as the feed. The substrate adopts RuiLong, and its dielectric constant is 2.2. **Figure 9a** shows the physical structure of the patch antenna. The parameters are pa = 4.5 mm, pb = 3.4 mm, and pl = 14 mm. To connect the adapter, two air holes with a radius of 1 mm are drilled on the substrate. **Figure 9b** shows the radiation pattern of the patch antenna at 25 GHz, and the realized gain is 7.3 dBi.

Establishing a CST Microwave Studio model. **Figure 10a** shows the phase distribution of the interferometric phase transmitarray, and **Figure 10b** shows the simulation model. **Figure 10c** and **d** illustrate the 3-D radiation patterns when the two feeds are excited respectively, and the realized gain of the proposed transmitarray antenna is 18.4 dBi at 25 GHz. Moreover, the radiation patterns shown in **Figure 10c** and **d** are symmetric about the yoz-plane.

The above results show that when multiple EM waves radiate toward the array, all the transmitted waves are formed into high-directivity beams. This process is characteristic of the transmitter of the MIMO system integrated by interferometric phase transmitarray. Next, analyze the characteristics of the receiver. When the plane wave illustrates the interferometric phase transmitarray vertically, the transmitted plane
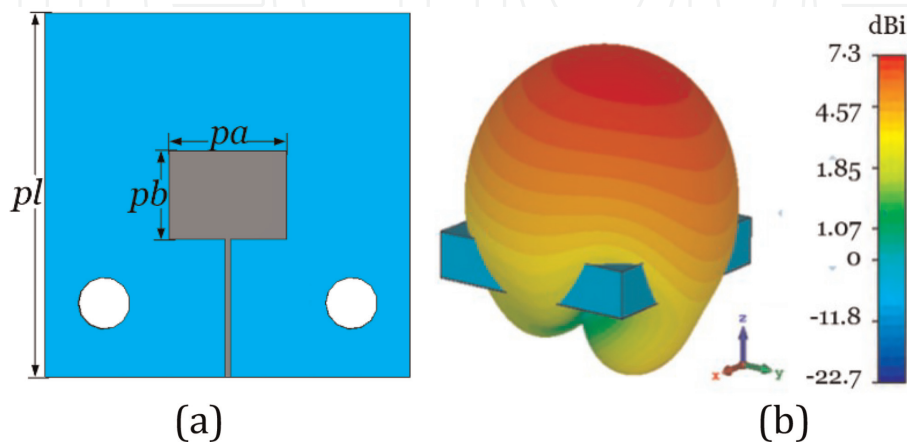

Figure 9.
(a) The physical structure of the patch antenna. (b) The simulated radiation pattern. Reprinted with permission from Ref. [22]; copyright 2022 IEEE.
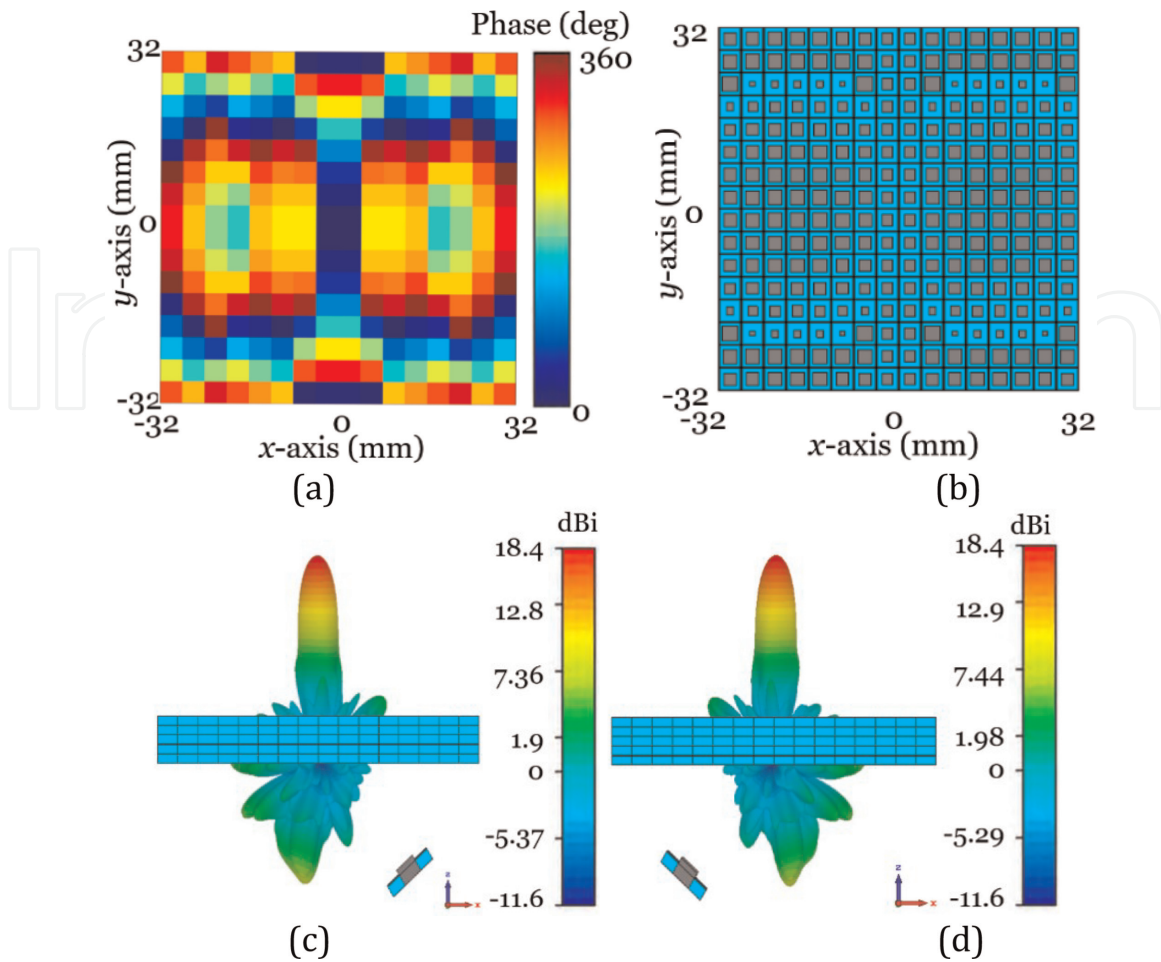
Figure 10.
(a) The Phase distribution of the interferometric phase transmitarray, (b) the CST Microwave Studio model, (c) when the right feed is excited, the 3-D pattern at 25 GHz, (d) when the left feed is excited, the 3-D pattern at 25 GHz. Reprinted with permission from Ref. [22]; copyright 2022 IEEE.
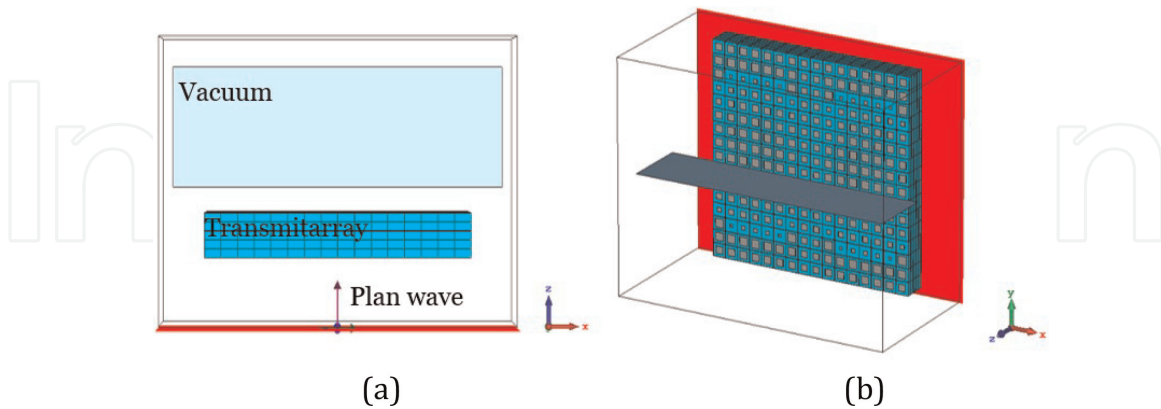

Figure 11.
Simulation setup in CST time-domain solver. (a) xoz plane view. (b) 3D view.

wave will be scattered and focused to two places. The proposed transmitarray is discretized and simulated using CST Studio Suite with the setup illustrated in **Figure 11**. Set the plane wave radiated along the z-axis to illuminate the transmitarray. A xoz plane square vacuum without thickness, as shown in **Figure 11a,** is set above the transmitarray to observe the focuses.
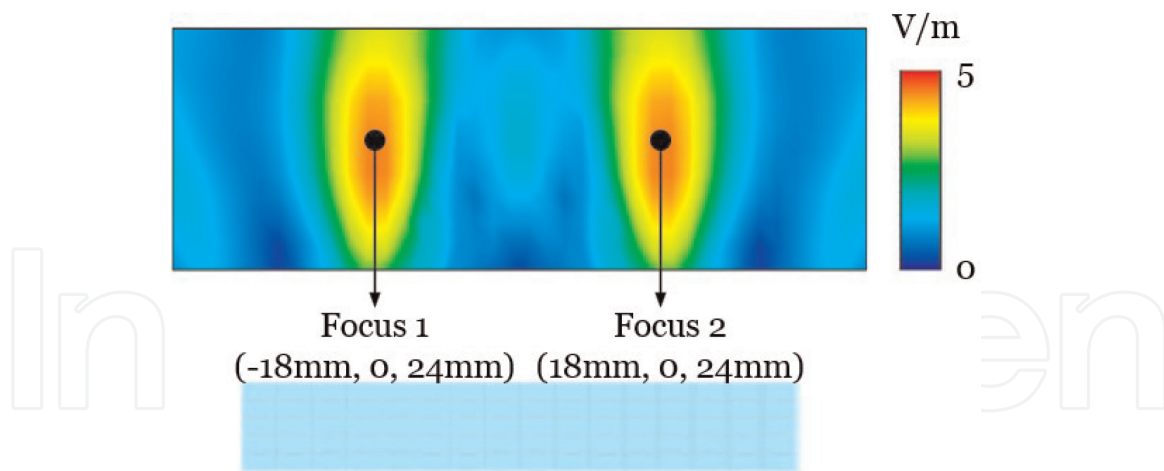
Figure 12.
The E-field distribution of the interferometric phase transmitarray under plane wave illumination.

Set up the e-field monitor and the simulated result is shown in **Figure 12**. It can be seen that when the plane wave illustrates the interferometric phase transmitarray vertically, the e-field will form two focuses, and its central coordinates are (-18 mm, 0, 24 mm) and (18 mm, 0, 24 mm).

In summary, when multiple EM waves radiate toward the transmitarray, all the EM waves are beamforming into high-directivity beams. When the plane wave illustrates the interferometric phase transmitarray vertically, the e-field will form two focuses, and its relative positions are consistent with the relative positions of the two feeds. These characteristics successfully enable the interferometric phase transmitarray to achieve the MIMO system, as shown in **Figure 2**.

4. Fabrication and experiment

To verify, a transmitarray and two patch antennas were fabricated. **Figure 13** shows that the prototype is verified in the anechoic chamber.
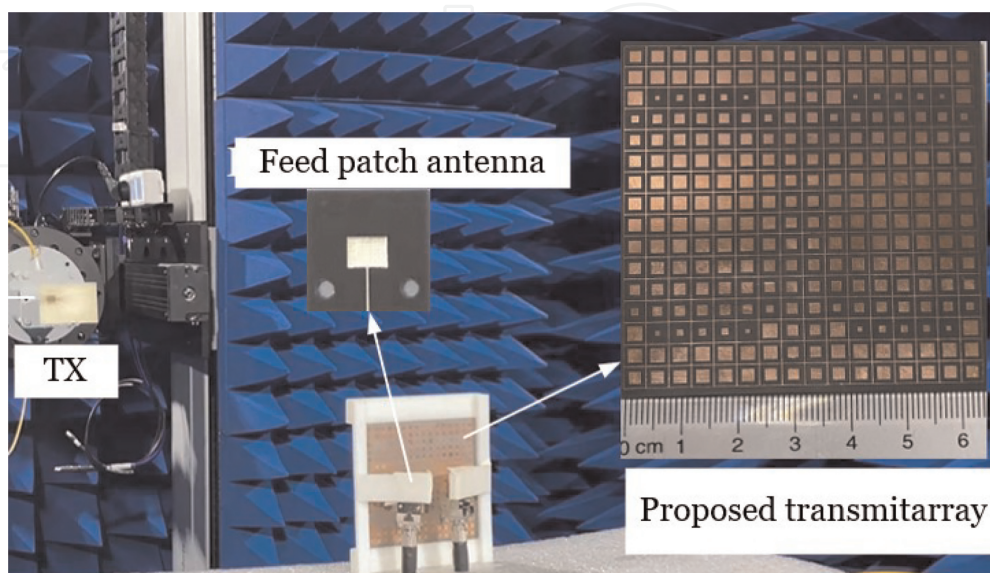

Figure 13.
The prototype is verified in the anechoic chamber. Reprinted with permission from Ref. [22]; copyright 2022 IEEE.
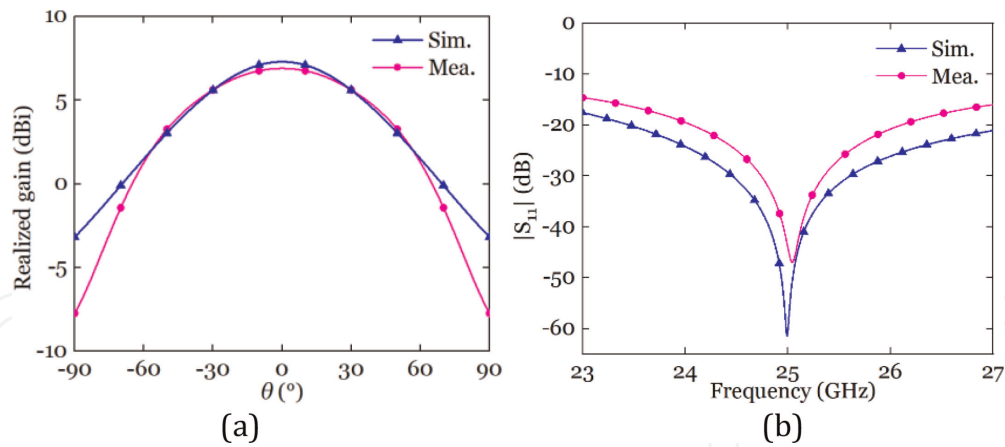
Figure 14.
(a) The simulated and measured patterns of the patch antenna at 25 GHz. (b) The simulated and measured $|S_{11}|$ of the interferometric phase transmitarray excited by the patch antenna. Reprinted with permission from Ref. [22]; copyright 2022 IEEE.

Figure 14a shows the patterns at 25 GHz of the patch antenna, and the simulated and measured curves are similar. **Figure 14b** shows the simulated and measured $|S_{11}|$ of the interferometric phase transmitarray excited by the patch antenna.

Figure 15 shows the simulated and measured patterns at 25 GHz of the interferometric phase transmitarray excited by the patch antenna. The simulated realized gain is 18.4 dBi, which is 0.9 dBi higher than the measured realized gain. In addition, the simulated and measured sidelobe level is around -15 dB, within a reasonable range. Minor differences between curves are mainly caused by the measurement environment.

5. MIMO behavior

To evaluate the performance of the proposed interferometric phase MIMO system, a same-size unifocal transmitarray antenna with a focus on (18 mm, 0, −30 mm) is introduced for simple comparison. **Figure 16** shows the simulated pattern.
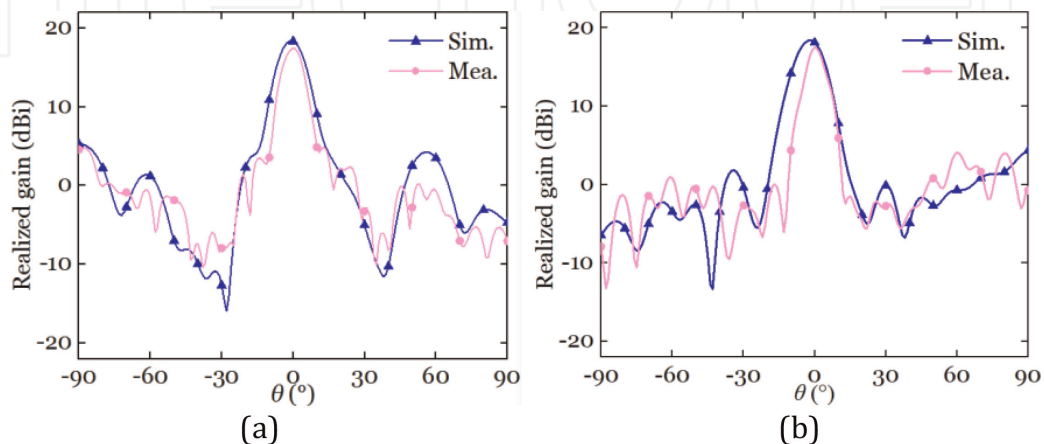

Figure 15.
The simulated and measured patterns at 25 GHz of the interferometric phase transmitarray excited by the patch antenna. (a) xoz-plane. (b) yoz-plane. Reprinted with permission from Ref. [22]; copyright 2022 IEEE.
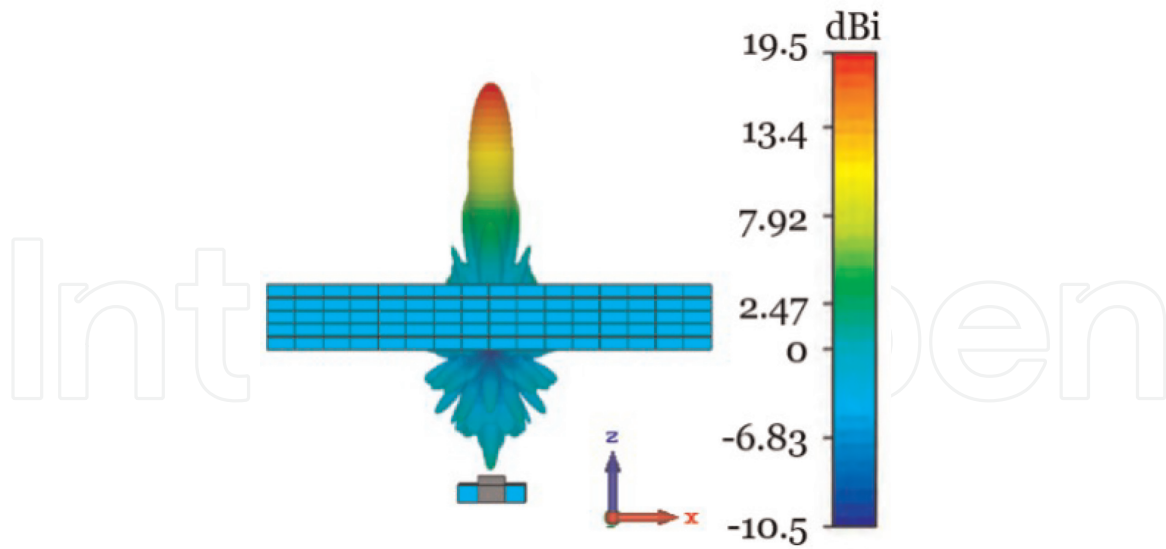
Figure 16.
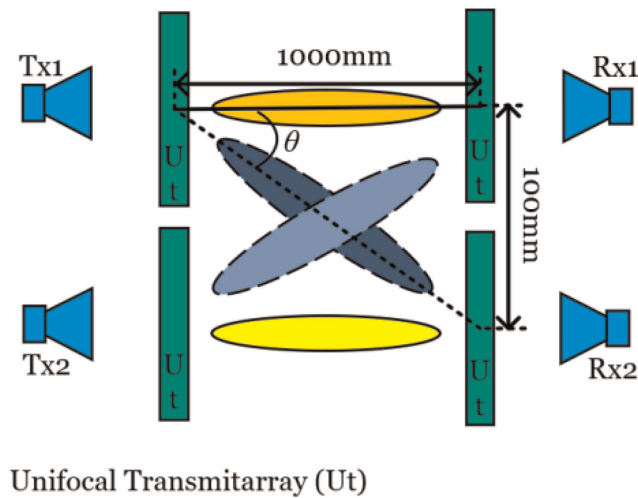*The simulated pattern of the unifocal transmitarray antenna at 25 GHz.*

Figure 17.
The simulated 3D pattern of the unifocal transmitarray antenna at 25 GHz.

Figure 17 shows the 2 × 2 MIMO system integrated by four unifocal transmitarray. It is assumed that the distance between two unifocal transmitarrays on one side is 100 mm and the transmission distance is 1000 mm, then the angle of the cross weak channels is θ = 6°. **Figure 18** shows the simulated xoz-plane pattern of the unifocal transmitarray antenna at 25 GHz. It can be seen from **Figure 18** that when θ = 6°, the gain is 15.2 dBi.

The channel capacity can be calculated by Eq. (7) as follows

$$C = B \log 2(1 + S/N) \tag{7}$$

where B is bandwidth, and S/N represents signal noise ratio. In MIMO links, the higher the receiving power, the greater the S/N, and the larger the channel capacity. The receiving power can be expressed as Eq. (8).

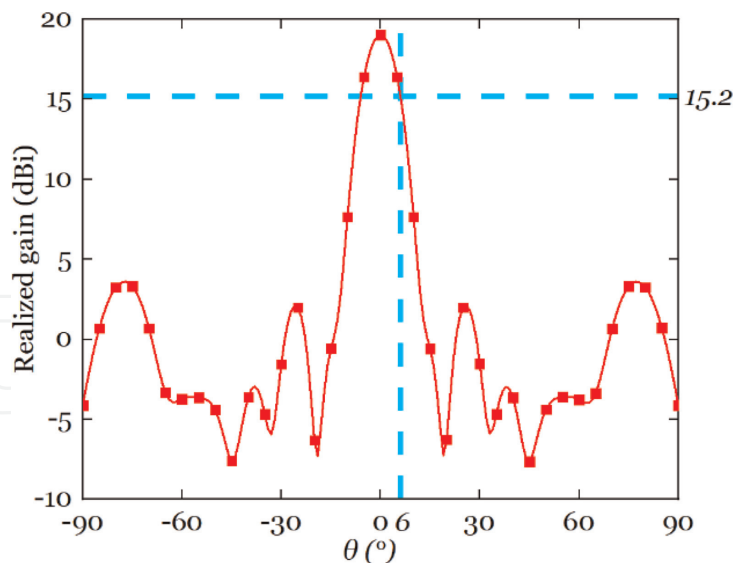$$P_r = P_t \frac{G_t G_r \lambda_0{}^2}{16\pi^2 d^2} \tag{8}$$

Figure 18.
The simulated xoz-plane pattern of the unifocal transmitarray antenna at 25 GHz.

where P_r and P_t represent receiving power and transmitting power, G_r and G_t represent the gain of the receiving antenna and the transmitting antenna, λ_0 is the wavelength in free space, and d is the distance between transmitter and receiver.

Therefore, the channel capacity is positively correlated with the gain of the receiving antenna and transmitting antenna. To compare the two MIMO systems in **Figures 1** and **2**, it is assumed that all environments are the same, except for antenna gain differences. The gains of the receiving and transmitting antennas in the 2×2 MIMO system integrated by interferometric phase transmitarray are all 18.4 dBi. Normalize the channel capacity of each link to 1, and the channel capacity of the 2×2 MIMO system is 4. By comparison, there are two strong channels and two weak channels in the 2×2 MIMO system in **Figure 17**. The gains of the receiving and transmitting antennas are 19.5 dBi in strong channels and 15.2 dBi in weak channels. In the 2×2 MIMO system in **Figure 17**, the 18.4 dBi of the antenna gain is still used to normalize the channel capacity. After normalization, the channel capacity of the strong channel is 1.056, and the weak channel is 0.823 in **Figure 17**. Therefore, the channel capacity of the 2×2 MIMO system in **Figure 17** is 3.758, which is lower than the 2×2 MIMO system integrated by interferometric phase transmitarray. In addition, the distance between transmitter and receiver d will also affect the channel capacity of the MIMO system in **Figure 17**. Since when d decreases, the angle of the cross weak channels θ increases, resulting in a decrease in antenna gain in weak channels. When d increases, the result is the opposite.

Therefore, through simple comparison, it can be found that the channel capacity of the 2×2 MIMO system integrated by interferometric phase transmitarray is higher than the 2×2 MIMO system integrated by unifocal transmitarray.

6. Conclusions

The proposed interferometric phase transmitarray can adjust two EM waves to the boresight of the transmitarray. When the plane wave illustrates the proposed transmitarray, the transmitted plane wave will be scattered and focused on two

positions. The MIMO system integrated by the interferometric phase transmitarray breaks the limitations of weak channels in conventional lens MIMO. In addition, the proposed method of the MIMO system can be extended to more channels.

Author details

Yu Luo* and Xiaoxuan Guo
Tianjin Key Laboratory of Imaging and Sensing Microelectronic Technology, School of Microelectronics, Tianjin University, Tianjin, China

*Address all correspondence to: yluo@tju.edu.cn

IntechOpen

References

[1] Almasi MA, Mehrpouyan H, Vakilian V, Behdad N, Jafarkhani H. A new reconfigurable antenna MIMO architecture for mmwave communication. In: Proceedings of the IEEE International Conference Communication (ICC). Kansas City, MO, USA. 2018. pp. 1-7

[2] Loyka S. The capacity of Gaussian MIMO channels under total and per-antenna power constraints. IEEE Transactions on Communications. 2017; **65**(3):1035-1043

[3] Li X et al. 120 Gb/s wireless terahertz-wave signal delivery by 375 GHz-500 GHz multi-carrier in a 2 × 2 MIMO system. Journal of Lightwave Technology. 2019;**37**(2):606-611

[4] Statnikov K, Grzyb J, Heinemann B, Pfeiffer UR. 160-GHz to 1-THz multi-color active imaging with a Lens-coupled SiGe HBT Chip-set. IEEE Transactions on Microwave Theory Technology. 2015; **63**(2):520-532

[5] Puerta R, Yu J, Li X, Xu Y, Vegas Olmos JJ, Tafur Monroy I. Single-carrier dual-polarization 328-Gb/s wireless transmission in a D-band millimeter wave 2 × 2 Mu-MIMO radio-over-fiber system. Journal of Lightwave Technology. 2018;**36**(2):587-593

[6] Zhang J, Yu J, Chi N, Dong Z, Li X, Chang G. Multichannel 120-Gb/s data transmission over 2 × 2 MIMO fiber-wireless link at W-band. IEEE Photonics Technology Letters. 2013; **25**(8):780-783

[7] Yang B, Yu Z, Lan J, Zhang R, Zhou J, Hong W. Digital beamforming-based massive MIMO transceiver for 5G millimeter-wave communications. IEEE Transactions on Microwave Theory Technogy. 2018;**66**(7):3403-3418

[8] Uwaechia AN, Mahyuddin NM, Ain MF, Abdul Latiff NM, Zabah NF. On the spectral-efficiency of low-complexity and resolution hybrid precoding and combining transceivers for mmwave MIMO systems. IEEE Access. 2019;**7**:109259-109277

[9] Yu C et al. Full-angle digital predistortion of 5G Millimeter-wave massive MIMO transmitters. IEEE Transactions on Microw. Theory Technology. 2019;**67**(7):2847-2860

[10] Darvazehban A, Ahdi Rezaeieh S, Zamani A, Abbosh AM. Pattern reconfigurable metasurface antenna for electromagnetic torso imaging. IEEE Transactions on Antennas and Propagation. 2019;**67**(8):5453-5462

[11] He Y, Ding N, Zhang L, Zhang W, Du B. Short-length and high-aperture-efficiency horn antenna using low-loss bulk anisotropic metamaterial. IEEE Antennas Wireless Propagation Letters. 2015;**14**:1642-1645

[12] Valentine J, Zhang S, Zentgraf T, Zhang X. Development of bulk optical negative index fishnet metamaterials: Achieving a low-loss and broadband response through coupling. Proceedings of the IEEE. 2011;**99**(10): 1682-1690

[13] Costa F, Genovesi S, Monorchio A, Manara G. Low-cost metamaterial absorbers for sub-GHz wireless systems. IEEE Antennas Wireless Propagation Letters. 2014;**13**:27-30

[14] Li H, Wang G, Xu H, Cai T, Liang J. X-band phase-gradient metasurface for

high-gain lens antenna application. IEEE Transactions on Antennas and Propagation. 2015;**63**(11):5144-5149

[15] Han J, Li L, Ma X, Feng Q, Zhao Y, Liao G. A holographic metasurface based on orthogonally discrete unit-cell for flexible beam formation and polarization control. IEEE Antennas Wireless Propagation Letters. 2021;**20**(10): 1893-1897

[16] Su Y, Chen ZN. A flat dual-polarized transformation-optics beamscanning Luneburg lens antenna using PCB-stacked gradient index metamaterials. IEEE Transactions on Antennas and Propagation. 2018;**66**(10):5088-5097

[17] Jia Y, Liu Y, Zhang W, Wang J, Gong S, Liao G. High-gain Fabry-Perot antennas with wideband low monostatic RCS using phase gradient metasurface. IEEE Access. 2019;**7**:4816-4824

[18] Xiao Y, Yang F, Xu S, Li M, Zhu K, Sun H. Design and implementation of a wideband 1-bit transmitarray based on a Yagi–Vivaldi unit cell. IEEE Transactions on Antennas and Propagation. 2021; **69**(7):4229-4234

[19] Aziz A, Yang F, Xu S, Li M. A low-profile quad-beam transmitarray. IEEE Antennas Wireless Propagation Letters. 2020;**19**(8):1340-1344

[20] Tao Z, Bao D, Xu HX, Ma HF, Jiang WX, Cui TJ. A Millimeter-wave system of antenna Array and metamaterial Lens. IEEE Antennas Wireless Propagation Letters. 2016;**15**: 370-373

[21] Jiang M, Chen ZN, Zhang Y, Hong W, Xuan X. Metamaterial-based thin planar lens antenna for spatial beamforming and multibeam massive MIMO. IEEE Transactions on Antennas Propagation. 2017;**65**(2):464-472

[22] Guo X, Luo Y, Chen ZN, Yan N, An W, Ma K. Interferometric phase Transmitarray for spatial power combining to enhance EIRP of Millimeter-wave transmitters. IEEE Transactions on Antennas and Propagation. 2022;**70**(11):10485-10493